Rheologica Acta (2024) 63:397–406
https://doi.org/10.1007/s00397-024-01451-1

ORIGINAL CONTRIBUTION

# Gelation of PU elastomers: rheological characterization for liquid additive manufacturing

**Peng Wang[1] · H. Henning Winter[2] · Manfred H. Wagner[1] · Dietmar Auhl[1]**

Received: 7 February 2024 / Revised: 26 March 2024 / Accepted: 12 April 2024 / Published online: 27 April 2024


## Abstract

Polyurethane (PU) is a versatile polymer with many applications in a wide range of products. A novel 3D printing technology called liquid additive manufacturing (LAM) extended its possibilities by generating PU elastomers with gradient properties in continuous processing. LAM, being a relatively new technique, has not been extensively researched, particularly in terms of the curing behavior of the liquid resin. In this work, we investigated the effect of composition on gelation time $t_{GP}$ as measured by time-resolved mechanical spectroscopy (TRMS) and analyzed using the Winter–Chambon criterion with the assistance of the IRIS software. This method is more accurate than the previous approach, which involved time sweeps with a constant frequency. It was found that the gel time $t_{GP}$ first decreased and then increased with increasing polyol ratio, ranging from 231 to 378 min. Furthermore, the crosslink densities of the different PU elastomers measured from the rheological and tensile tests were calculated and compared based on the theory of rubber elasticity. The crosslink density decreased with an increasing polyol ratio in both methods. However, the crosslink density values obtained from the rheological measurements were higher than those from the tensile tests. These findings demonstrate that adjusting the polyol ratio is an effective means of achieving gradient properties. The composition effects we measured offer valuable insights for the design of LAM–PU elastomers.

**Keywords** Polyurethane · Liquid additive manufacturing · Gelation · Time-resolved mechanical spectroscopy · Crosslink density

## Introduction

Polyurethane (PU) is a polymer material that was first produced by Otto Bayer in 1937 (Bayer 1947). Over time, two major types of PU materials emerged: polyester type and polyether type (Nakajima-Kambe et al. 1999). They can be transformed into various forms, including thermoplastic, rubber, and elastomer, depending on their intended usage (Somarathna et al. 2018). PU materials can be made either rigid or flexible, depending on the starting materials and reaction conditions. PU finds a wide range of applications, such as insulation, coatings, adhesives, foam, fiber, and even furniture. Its resistance to water, oil, grease, chemicals, and bacteria makes PU suitable for use in harsh environments. Its high abrasion resistance, cut and tear resistance, load-bearing capacity, and colorability make PU an ideal choice for wear-resistant parts and products that require durability and aesthetics. Depending on its reactants and molecular weight, polyurethanes can be either thermosetting with controlled crosslink density or thermoplastic. All of these characteristics make polyurethane a versatile material, opening up a wide range of possibilities due to its capability of adjusting its properties, mostly by controlling the crosslinking reaction.

Additive manufacturing (AM) is one of the technologies that have grown the most in the last decade or so. AM refers to the process of joining materials and manufacturing objects from 3D model data, usually layer by layer (Huang et al. 2013). Based on the ISO/ASTM 52900 standard, AM includes seven main processing techniques, which are material extrusion, vat polymerization, powder bed fusion,

✉ Peng Wang
peng.wang.1@tu-berlin.de

[1] Department of Polymer Materials and Technologies, Technische Universität (TU) Berlin, Ernst-Reuter-Platz 1, 10587 Berlin, Germany

[2] Department of Chemical Engineering and Polymer Science & Engineering, University of Massachusetts, Amherst, MA 01003, USA

material jetting, binder jetting, direct energy deposition, and sheet lamination (Jandyal et al. 2022).

In this context, we are focusing on liquid additive manufacturing (LAM), a promising new technology that enables the production of 3D objects from liquid raw materials capable of undergoing crosslinking with local composition variations. These materials consist of crosslinking components, which are mixed shortly before being ejected through the printing nozzle. During the flow through the printing nozzle, the PU mixture is still in the liquid state, but it then undergoes a crosslinking reaction during the remainder of the printing process. This reaction provides essential structural support for the printed part, allowing for the addition of further layers. It is crucial to determine the minimum time required for the liquid raw materials to solidify sufficiently through crosslinking to maintain the stable shape of the currently deposited layer. Due to these considerations, during the LAM process of PU elastomers, understanding the gel time of the liquid raw materials becomes vital. The gel time determines the minimum waiting period before applying the next layer on top of the previous one.

On the other hand, the deposition of the next layer should not be much later than the gel time. This guarantees molecular connectivity between layers due to high molecular mobility at the instant of deposition.

Rheological characterization of the material during crosslinking can be employed to ascertain the time required to reach the gel point, commonly referred to as the "gel time". Chemo-rheology describes the rheological behavior of cross-linked polymers during chemical reactions, such as curing or vulcanization. The changes in the flow behavior of cross-linked polymers are monitored through rheological measurements during the curing reaction, making it one of the most direct methods for detecting the gel point (Osswald and Rudolph 2015).

Time-resolved mechanical spectroscopy (TRMS) (Mours and Winter 1994) is a rheological measurement technique that has been widely utilized for characterizing materials undergoing structural changes, such as gelation, phase transitions, decomposition, and polymerization (Kruse and Wagner 2016, Kruse 2017, Arrigo et al. 2020, Salehiyan et al. 2017, Salehiyan et al. 2019, Laukkanen et al. 2018, Takeda et al. 2020). TRMS measurements consist of a series of cyclic frequency sweeps which yield data on the storage modulus ($G'$) and loss modulus ($G''$) as functions of reaction time. The moment when $G'$ and $G''$ linearize at low frequencies and become parallel is referred to as the "gel time". Gel time signifies the transition from a liquid to solid state.

There are some more qualitative ways of estimating the gel point of crosslinking materials (Schäfer et al. 2020, Djabourov and Nishinari 2013, Hu et al. 2001). The simplest way to estimate the gel time by rheological measurement is by steady shear rheometry. This method probes the growth of viscosity as the sample approaches the gel point. Initially, the viscosity of the sample is very low. As the curing reaction progresses, the viscosity gradually increases until it reaches a high value. Consequently, stress also increases and causes some internal fracturing, which delays the expected divergence of the viscosity. Because of this, the viscosity-determined "gel point" of the partially broken sample suggests a gel time that is too long.

Another way to estimate the gel point is by using small amplitude oscillatory shear (SAOS) at a constant oscillation frequency and attributing the crossover point of the storage modulus ($G'$) and the loss modulus ($G''$) as the gel point (Tung and Dynes 1982). It was originally believed that the gel point occurred when $G'$ equals $G''$, according to ASTM D4473. At the crossover point of $G'$ and $G''$, the energy stored equals the energy dissipated during deformation. This method may be valid for certain types of polymers (Mortimer et al. 2001). However, it cannot be applied reliably due to the strong frequency dependence of the crossover point (Winter 1987).

In this study, we investigated the gel time of five polyurethane (PU) systems with varying polyol ratios using time-resolved mechanical spectroscopy (TRMS). Different polyol ratios lead to distinct structures, which, in turn, influence the material properties. The primary properties examined include gel time and the degree of crosslinking, assessed through rheological measurements. Consequently, we obtained a reference time for the liquid additive manufacturing (LAM) process, indicating when the next layer can be printed atop the preceding one.

## Theoretical background

### Flow behavior of curing reaction

The gel point, also recognized as GP or critical gel, within a chemically crosslinking polymer, occurs when the weight average molecular weight reaches an infinite value (Flory 1941). The gel point can also be classified as the transition from the liquid to solid state. The dynamic moduli $G'$ and $G''$ can be used to characterize the gel point due to the easily detectable power law relaxation modulus $G(t) = St^{-n}$, which governs viscoelasticity at the gel point (Winter 1987).

One of the typical linear viscoelastic features of critical gels is that the long tail of the relaxation time spectrum is self-similar and can be expressed by a power law with gel strength S and relaxation exponent values ($-n_c$) between $-1$ and 0, depending on material details.

Combining small amplitude oscillatory shear (SAOS) data with the two material parameters for GP (S and $-n_c$), the general constitutive equation of linear viscoelasticity results in a

constitutive equation for critical gels, the Winter–Chambon gel equation:

$$\underline{\sigma}(t) = S\int_{-\infty}^{t} dt'\left(t-t'\right)^{-n_c}\underline{\dot{\gamma}}(t') \tag{1}$$

$\sigma(t)$ and $\dot{\gamma}(t')$ are the stress and rate of strain tensor (Winter 2016).

At the transition state of the crosslinking process, when $t = t_{GP}$, the phenomenon of $G^{'}$ and $G^{''}$ being parallel to each other defines the gel point of materials. As a result, tanδ becomes independent of frequency. This parallel orientation of $G^{'}$ and $G^{''}$ is caused by the power law format of the relaxation modulus.

During gelation, changes in the sample structure lead to significant variations in $G^{'}$ and $G^{''}$. However, as long as these changes are small when acquiring a single data point, the evolution of connectivity can be approximated as a sequence of quasi-stable states and described using classical linear viscoelasticity (Mours and Winter 1994). The mutation time, introduced as an expression of the instantaneous rate of change, serves as the characteristic time constant for the mutation process,

$$\lambda_{mu} = \left[\frac{1}{g}\frac{\partial g}{\partial t}\right]^{-1} \tag{2}$$

$$N_{mu} = \frac{\Delta t}{\lambda_{mu}} \tag{3}$$

The mutation number $N_{mu}$ (Winter et al. 1988) estimates the change that occurs during the acquisition of a single data point at a small amplitude oscillatory shear (SAOS) period of $2\pi/\omega$ and provides a criterion to estimate the magnitude of this effect. For instance, $N_{mu}=0.1$ indicates a 10% change for that specific data point, which is considered an acceptable value. In this case, variable $g$ is the property of interest (i.e., $G'$, $G''$), and $\Delta t$ is the duration of a single measurement. In TRMS, $\Delta t$ is approximately obtained by the time required for the rheometer to take a data point at the specified angular frequency $\omega$.

$$\Delta t = \frac{2\pi}{\omega} \tag{4}$$

Based on Eq. (3), the mutation number can be calculated for $G'$ and $G^{''}$, as follows:

$$N^{'}_{mu} = \frac{2\pi}{\omega G'}\frac{\partial G'}{\partial t}N^{''}_{mu} = \frac{2\pi}{\omega G^{''}}\frac{\partial G^{''}}{\partial t} \tag{5}$$

## Rubber elasticity and crosslinking density

Rubber elasticity is the ability to fully recover after being subjected to very large deformations. Many polymer materials consisting of long crosslinking molecular chains exhibit such properties. Based on the thermodynamics of rubber, the entropy change ($\Delta S_{net}$) is the feature of rubber elasticity during deformation (Rubinstein and Colby 2003).

$$\Delta S_{net} = -\frac{nk}{2}(\lambda_x^2+\lambda_y^2+\lambda_z^2-3) \tag{6}$$

$n$ is the number of strands in a network, $k$ is the Boltzmann constant, and λ is the deformation factors for x, y, and z directions, which equals undeformed dimension over deformed dimension.

Ignoring any enthalpic contribution, the change of free energy ($\Delta F_{net}$) is

$$\Delta F_{net} = -T\Delta S_{net} = \frac{nkT}{2}(\lambda_x^2+\lambda_y^2+\lambda_z^2-3) \tag{7}$$

$T$ is the absolute temperature.

If the network is uniaxially deformed (e.g., x-direction) at constant volume (V), the deformation factors are

$$\lambda_x = \lambda \qquad \lambda_y = \lambda_z = \frac{1}{\sqrt{\lambda}} \tag{8}$$

and the free energy change for uniaxial deformation is

$$\Delta F_{net} = \frac{nkT}{2}(\lambda^2+\frac{2}{\lambda}-3) \tag{9}$$

As a result, the stress in the x-direction is equal to the force over the cross-sectional area,

$$\sigma_{xx} = \frac{f_x}{L_yL_z} = \frac{\left(\frac{\partial \Delta F_{net}}{\partial L_x}\right)}{L_yL_z} = \frac{nkT}{V}(\lambda^2-\frac{1}{\lambda}) \tag{10}$$

and the extensional modulus is

$$E_{xx} = \frac{\partial \sigma_{xx}}{\partial \lambda} = \frac{3nkT}{V} \tag{11}$$

Assuming the Poisson's ratio equals 0.5, the extensional modulus is three times higher than the shear modulus.

$$G = \frac{E_{xx}}{3} = \frac{nkT}{V} = n_G R_g T \tag{12}$$

$n_G$ is the number of network strands per unit volume (crosslink density), and $R_g$ is the gas constant ($R_g = kN_A$, $N_A$ is the Avogadro number).

The storage modulus ($G'$) measured at the rubber plateau is usually used to calculate the crosslink density (Jiang et al. 1999).

$$G'_e = n_{G'_e}R_gT \tag{13}$$

Two other methods for estimating crosslink density are the equilibrium swelling method and stress–strain data. The

equilibrium swelling method is based on measuring the volume fraction of the polymer material in the equilibrium swelling state, which is shown as the Flory–Rehner equation (Hagen et al. 1996; Saville and Watson 1967)

$$-\ln\left(1-\nu_r\right)-\nu_r-\chi\nu_r^2=2V_0n_{\text{swell}}\left(\upsilon_r^{1/3}-\frac{\upsilon_r}{2}\right) \tag{14}$$

$\nu_r$ is the volume fraction of polymer in the swollen mass, $\chi$ is the polymer–solvent interaction parameter, $V_0$ is the molar volume of solvent, and $n_{\text{swell}}$ is the crosslink density.

The stress–strain data can also be used for the estimation of crosslinking density. It is based on the so-called Mooney–Rivlin equation (Sekkar et al. 2007).

$$\frac{\sigma}{\lambda-\lambda^{-2}}=2\mathrm{C}_1+\frac{2\mathrm{C}_2}{\lambda} \tag{15}$$

where σ is the extension force and λ is the extension ratio. $2C_2$ is the slope in the plot of $\sigma/\lambda-\lambda^{-2}$ versus $\lambda^{-1}$ and the intercept of the curve correspond to the value of $2C_1$, which is the parameter used to calculate the crosslinking density by use of Eq. (16).

$$n_{C_1}=\frac{C_1}{R_gT} \tag{16}$$

Due to the lack of corrections for chain ends, main-chain scission, and trapped chain entanglements, the storage modulus method has quantitative errors in calculating the crosslink density compared to the other two methods. Nevertheless, the storage modulus method is still used to estimate the crosslink density.

## Experimental

### Materials

In this study, two polyols (Lupranol L1100 and Lupranol L3300, BASF polyurethanes GmbH) and one polyisocyanate (Lupranat M20S, BASF polyurethanes GmbH) were used as the main reactants and diluted by anhydrous toluene (Sigma-Aldrich). The physical properties of all reactants can be found in the previous paper (Wang et al. 2019).

### Sample preparation

All reactants and preparation tools were placed in a vacuum oven at 60 °C for 24 h to dry as much as possible. After 24 h, Lupranol L1100, Lupranol L3300, and Lupranat M20S were firstly diluted by anhydrous toluene of 30 wt.%, 32 wt.%, and 25 wt.%, respectively. Table 1 shows the mass fraction of reactants for different polyol ratios, and the PU systems without catalysts were prepared.

### Rheological measurements

After preparation, each sample was promptly transferred to the rheometer, an Anton Paar MCR 301 equipped with a CTD 450 oven, consisting of two parallel disposable plates with a 25-mm geometry. The sample was placed onto the bottom plate using a pipette, and the top plate was then lowered to maintain a gap distance of 1.6 mm. The oven temperature was maintained at 30 °C.

The TRMS measurements ranged from 0.5 to 500 rad/s with 5 points per decade for each run. The strain amplitude was set to 0.5%. The TRMS consisted of 60 consecutive SAOS runs spanning almost 26 h and continued until the storage and loss moduli reached relatively stable saturation values.

### Tensile testing

After homogeneous mixing, the PU reactants dripped into a mold, slowly to avoid bubble formation. The mold with the liquid reactant was then placed into a freezer and stored for 24 h at a temperature of about 5 °C. During this time, the mold was transferred to a vacuum oven for degassing. All these steps were necessary to avoid bubble formation as much as possible. After 24 h, the mold and samples were removed from the freezer and cured at 30 °C for other 24 h. Thereby the specimen solidified and obtained a stable shape which allowed mechanical testing. Then the specimens were demolded and placed in an oven at 90 °C for 2-h post-curing. Tensile tests were carried out in a Zwick Z1446 machine. The specimen was stretched longitudinally on the tensile test machine at a rate of 50 mm/min to determine the stress–strain diagrams. A strain of up to 2% was used to determine the tensile modulus value.

**Table 1** Mass fraction of reactants for different polyol ratios ($PR=\frac{m_{L1100}}{m_{L1100}+m_{L3300}}$)

| PU system | Polyol ratio [%] | L1100 | L3300 | M20S | Hard segment fraction |
|---|---|---|---|---|---|
| | | [wt. %] | | | [-] |
| PU-00 | 0.00 | 0 | 50.04 | 49.96 | 0.50 |
| PU-17 | 0.17 | 9.08 | 44.32 | 46.60 | 0.47 |
| PU-33 | 0.33 | 19.03 | 38.05 | 42.92 | 0.43 |
| PU-50 | 0.50 | 30.69 | 30.69 | 38.62 | 0.39 |
| PU-66 | 0.66 | 44.27 | 22.14 | 33.59 | 0.34 |

## Results and discussion

Figure S1 in the supplementary information is the measuring plot from the rheometer for PU-00 and PU-66, where (a) is G′ and G′′ as a function of time and (b) is the complex viscosity as a function of time. The measured values of G′ are not stable and do not show a consistent trend in the first 4 h, because the sample at the beginning is a low-viscous liquid ($\eta \approx 10^{-1} \sim 10^{-2}$Pa • s). The value of G′′ is a feature of this behavior and dominates in the early stages of the reaction (Elwell et al. 1996).

As the reaction progresses, when G′ and G′′ are gradually parallel to each other and the values are similar i.e., the ratio of G′′ and G′, tanδ is independent of frequency, this refers to the gel point. This can help us to estimate preliminarily the gel point of each PU system. After the transition phase, G′ becomes larger than G′′, which means that the elastic part dominates over the viscous part due to the crosslinking of the sample.

In Fig. S1 (b), the values show a downward trend in each frequency sweep test due to shear thinning. The shear thinning effect becomes more and more obvious as the crosslinking reaction progresses. Overall, the viscosity values increase significantly and then reach a plateau.

These plots provide a wealth of information about the rheology and kinetics of the samples. The data measured (frequency, G′, G′′, and time) from the rheometer are exported and analyzed by the software IRIS (Winter and Mours 2006).

### Gel point of pure PU samples by TRMS

In the work of Winter et al. (1988) and Mours and Winter (1994) when $N_{mu}$ is smaller than 0.15, the condition can be considered a quasi-stable state. Furthermore, an analysis in 1994 resulted in a critical mutation number $N_{mu}$= 0.9 for the non-isothermal case beyond which the material response became non-linear. In Table 2 , the $\Delta t$ is obtained from the measurements in rheometer, which records the time interval for the data points from each frequency. The results indicate that all PU samples are in a quasi-steady state.

The change of G′ is more sensitive to structural change compared to G′′; therefore, the property of interest $g$ is used as G′ to demonstrate mutation time $\lambda'_{mu}$. Then, Eq. (2) can be changed to Eq. (17).

$$\lambda'_{mu}{}^{-1} = \left[\frac{1}{G'}\frac{\partial G'}{\partial t}\right] = \left[\frac{\partial \ln G'}{\partial t}\right] \tag{17}$$

In Fig. 1a–e, the black dashed lines serve as a reference for the gel point. The reaction time increases for each curve from top to bottom. Curves positioned above the black dashed line represent the pre-gelation stage, while those below it indicate the post-gelation stage. The reaction time of the curve closest to the black dashed line designates the gelation time for these samples, as indicated by a star (*) in the figure. For most samples, G′′ still dominates at the gel point. The material assumes a soft solid state where G′′ dominates, which is advantageous since newly printed layers can adhere to preceding ones. Only well beyond the gel point, in the post-gelation state, elasticity becomes more pronounced, with G′′ significantly lower than G′, leading to tan$\delta$ values less than 1.

**Table 2** Mutation number for each PU sample at different frequencies

| PU | Frequency [rad/s] | 0.5 | 5 | 50 | 500 |
|---|---|---|---|---|---|
| | Δt[s] | 49.6 | 13.2 | 11.8 | 10.4 |
| PU-00 | $\lambda'_{mu}{}^{-1}$[$10^{-4}$ 1/s] | 7.19 | 5.85 | 4.95 | 4.51 |
| | $N'_{mu}$ | 0.036 | 0.008 | 0.006 | 0.005 |
| PU-17 | $\lambda'_{mu}{}^{-1}$[$10^{-4}$ 1/s] | 12.09 | 9.79 | 8.41 | 6.72 |
| | $N'_{mu}$ | 0.060 | 0.013 | 0.010 | 0.007 |
| PU-33 | $\lambda'_{mu}{}^{-1}$[$10^{-4}$ 1/s] | 10.29 | 9.28 | 7.53 | 6.54 |
| | $N'_{mu}$ | 0.051 | 0.012 | 0.009 | 0.007 |
| PU-50 | $\lambda'_{mu}{}^{-1}$[$10^{-4}$ 1/s] | 11.61 | 8.84 | 5.11 | 2.42 |
| | $N'_{mu}$ | 0.058 | 0.012 | 0.006 | 0.003 |
| PU-66 | $\lambda'_{mu}{}^{-1}$[$10^{-4}$ 1/s] | 8.15 | 7.16 | 4.15 | 1.64 |
| | $N'_{mu}$ | 0.040 | 0.009 | 0.005 | 0.002 |

Figure 1f summarizes the gelation time of the above five samples. Increasing the ratio of polyols leads to an initial decrease in gel time, followed by a subsequent increase. This is because the PU-00 exclusively incorporates triols in the reaction, resulting in a higher number of crosslinks in its structure compared to other PU samples. It is known that the molecular mass of triol is lower than that of diol, so it can be estimated that the chain length of triol is smaller than that of diol. In the absence of diols, triols react with polyisocyanates to form a relatively dense network structure that inhibits the moveability of some molecules. From a macroscopical aspect, the high viscosity produced by the crosslinking reaction slows down the reaction rate. In addition, triols contain only secondary hydroxyl groups, and the reaction rate also decreases. Therefore, PU-00 takes more time to reach the gel point. However, due to the formation of a dense network of crosslinked structures, PU-00 exhibits the highest storage modulus at the gel point, which can be seen in Fig. 2.

The viscosity of the PU polymers decreases as the ratio of diols increases because diols have relatively low viscosity, and they contain primary hydroxyl groups that can react earlier with a polyisocyanate to form a long linear chain and a crosslinked network. As shown in Fig. 2, the G′ of PU-17 is approximately 10 times lower than that of PU-00. With fewer inhibiting factors in the reaction system, the gel time is also lower, as observed in PU-17 and PU-33.

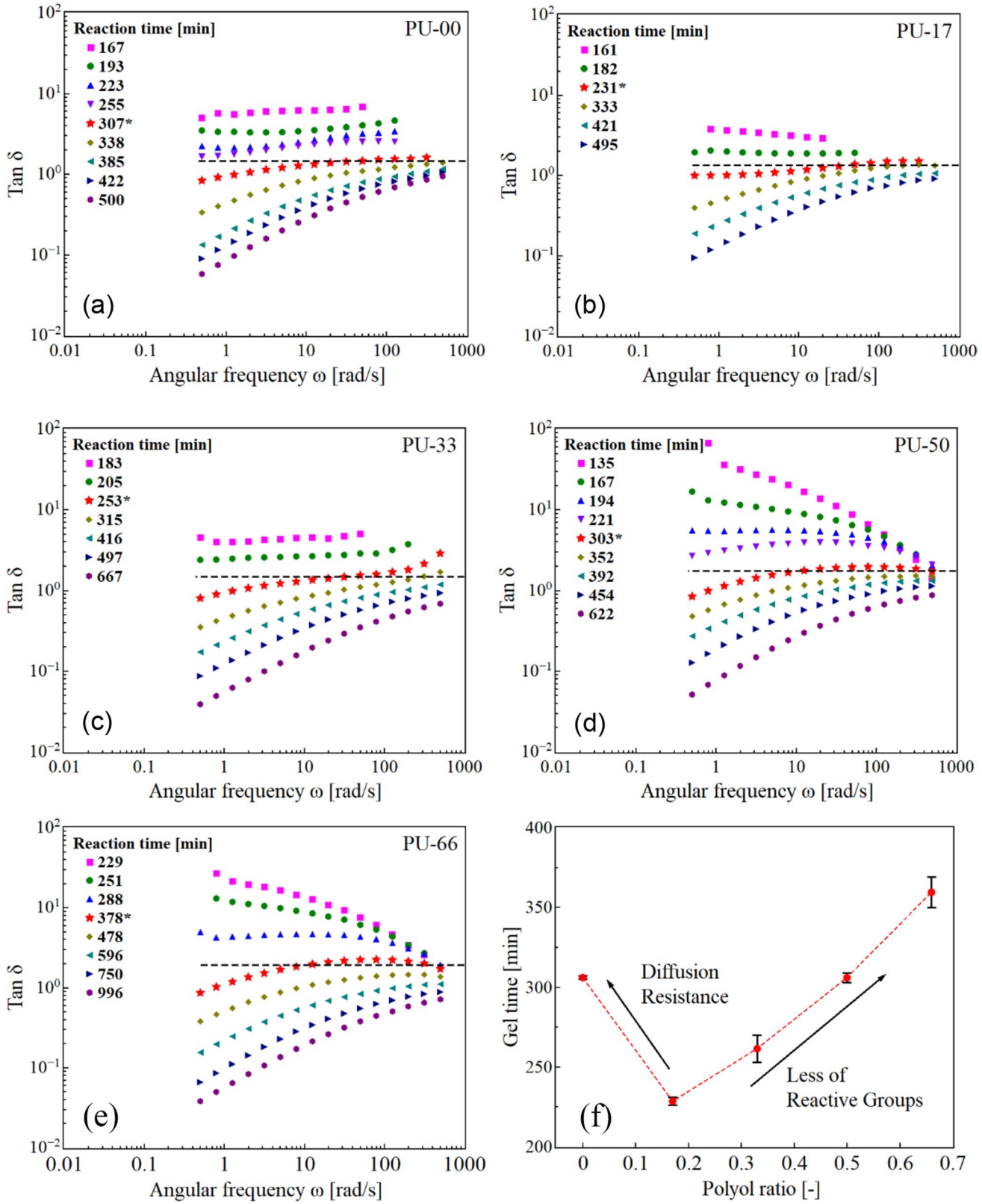


**Fig. 1** Loss factor as a function of angular frequency (**a**–**e**), and gel time for each PU sample (**f**) determined by interpolation of SAOS experiments using the IRIS software (Winter and Mours 2006)

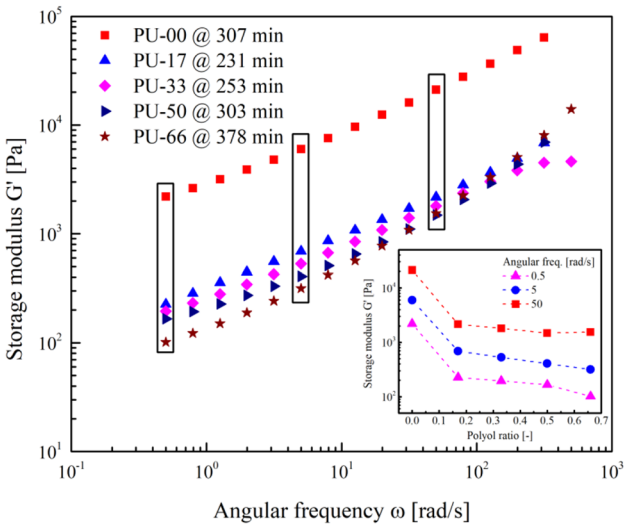


**Fig. 2** Storage modulus of each PU sample at the gel time and comparison at the angular frequency of 0.5, 5, and 50 rad/s

However, the addition of more L1100 (i.e., for PU-50 and PU-66) to the reaction dilutes the reaction system and hinders the reaction between triol and polyisocyanate, and the formation of a network structure is relatively slow. Therefore, the gel time of PU-50 and PU-00 is relatively the same again, and it takes the longest time for PU-66 to reach the gel point.

It should be noted that the gel time is an approximate value indicating the period of gelation. In the analysis, the TRMS data are used to estimate first the approximate gel point where the values of G′ and G″ are closest to each other, and then an interpolation is performed every 20 min. As a result, the interpolation curves with a time difference of less than 20 min are very similar. These curves are compared, and the curve of tan$\delta$ that is almost horizontal and close to the value of 1 is selected as the gel point.

## Crosslink density

Due to the different amounts of triol added to the reaction, the crosslinked structure of samples with different polyol ratios (PR) is expected to be different. Although all samples formed a network structure, the crosslink density, the number of entanglements, and the number of free chain ends are all related to the content of triol. This is true, especially for the crosslink density, which directly affects the performance of the material. Hagen et al. (1996) found that the crosslink density estimated by the storage modulus is higher than the value of the equilibrium swelling and stress–strain data. In this section, the storage modulus method and the stress–strain method are used to evaluate the crosslink density.

In the storage modulus method, all data are taken from the samples reacted in the rheometer for about 24 h. At this time, the conversion rate measured by FITR is greater than 90% as shown in Table 3. The measurement with FTIR and calculation of conversion can be seen in the previous work (Wang et al. 2019).

The storage modulus of samples with different PRs for 24 h is shown in Fig. 3. Each G′ curve increases with increasing angular frequency. When the frequency is less than 1 rad/s, it shows a plateau area. By extrapolating the plateau area to the Y-axis, the approximate value at 0 rad/s can be obtained. It is reasonable that the value of G′ at 0 rad/s decreases with the increase of PRs.

According to the intersection value on the ordinate in Fig. 3, the crosslink density can be calculated using Eq. (13). The crosslink density is shown in Fig. 6. The crosslink density decreases with increasing PR value. This is because, in samples with higher PR values, more diols are added to the reaction system, and the linear chain between every two crosslinking points is longer. However, PR-00 does not contain any diol, so the crosslink density is the highest. There is a nearly a factor of 7 times difference between PU-00 and PU-66.

**Table 3** Comparison of conversion of NCO for samples in the rheometer and tensile test

| PRs | Conversion of NCO in rheometer at 24 h | Conversion of NCO for the tensile test with post-cured at 2 h |
|---|---|---|
| PR-00 | 95.4% | 93.7% |
| PR-17 | 91.2% | 91.4% |
| PR-33 | 91.0% | 91.2% |
| PR-50 | 92.3% | 92.3% |
| PR-66 | 93.2% | 88.8% |

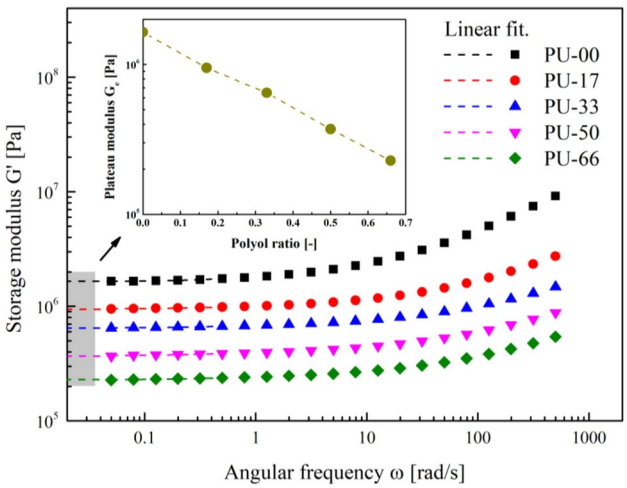


**Fig. 3** Storage modulus of PU samples with different PRs reacted in rheometer for 24 h. Dash lines are linear extrapolations to intercept

Using the information measured by FTIR, the conversion of the NCO group of each PR reacted in the rheometer for 24 h can be estimated. Similarly, the FTIR of the dumbbell-shaped sample used for the tensile test was also measured.

From Table 3, it can be seen that except for PU-66, which has a difference of about 5%, the conversion values of other samples post-cured within 2 h are relatively comparable to the conversion values of the samples that reacted in the rheometer for 24 h. Therefore, these tensile test data can be used to calculate the crosslink density and the calculated crosslink density can be compared. The stress–strain curves of each PU sample post-cured for 2 h are shown in Fig. 4.

With the increase of PRs, the samples become soft and tough, the stress at break becomes smaller, and the strain at break becomes larger. In the stress–strain curve, the stress increases faster when the strain is relatively small, but after the strain is larger than 5%, the stress increases slowly and roughly linearly. Therefore, the calculation of the crosslinking density mainly focuses on the strain greater than 10%, i.e., $\lambda^{-1}$ is less than 0.9.

However, according to Saville and Watson (1967), an elongation ratio λ of up to 2 is preferred, i.e., the elongation reaches more than 100%, but in all PU samples investigated, the maximum elongation is about 40% and $\lambda^{-1}$ about 0.7. According to the research of Mullins and Tobin (1965) on filler-reinforced vulcanized rubber, due to the presence of the filler, the ratio of the average strain to the measured overall strain is derived from the following factor.

$$X = 1 + 2.5x + 14.1x^2 \tag{18}$$

$x$ is the fraction of fillers.

$X$ Is a factor used to analyze simple tensile stress–strain data obtained at larger strain. For this reason, the Mooney–Rivlin relationship can be used to describe the behavior of the rubber.

Spathis (1991) mentioned that the presence of hard segments in PU material that are regarded as fillers prevent the soft matrix from deforming uniformly, resulting in an overall lower apparent strain than the locally occurring strains. The ratio of stress to strain is increased by factor X which accounts for both this disturbance of the strain distribution and the absence of deformation in the fraction of hard domains at the initial elongations. Therefore, $x$ of Eq. (18) can be the hard segment fraction which is listed in Table 1. The modified elongation ratio Λ and Mooney–Rivlin equation are shown in Eq. (19) and (20).

$$\Lambda = 1 + X\varepsilon \tag{19}$$

$$\frac{\sigma}{\Lambda - \Lambda^{-2}} = 2C_1 + \frac{2C_2}{\Lambda} \tag{20}$$

After correcting the data from Fig. 4 with strain amplification factor $X$, these examples all show some linear trends, and $\Lambda^{-1}$ reaches about 0.4. Therefore, the Mooney–Rivlin equation can be used for PU-00 to PU-66. Figure 5 shows the relationship between $\sigma/(\Lambda - \Lambda^{-2})$ and $\Lambda^{-1}$.

The linear fitting range of each curve starts from 0.4 to 0.6, because the curve of PU-00 turns up when $\Lambda^{-1}$ is larger than 0.6, resulting in a larger fitting slope. Since the strain of PU-00 is less than 25%, this is the reason why the slope of the linear fit is steeper than others, resulting in a relatively small intercept. Therefore, the crosslink density calculated by this method is relatively low. On the other hand, the slopes of PU-50 and PU-66 after strain amplification are negative, so the intercept is increased. Therefore, the crosslink density calculated by this method is relatively high.

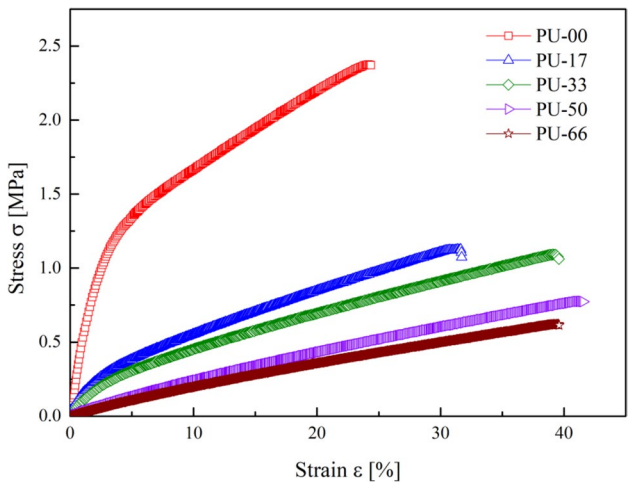


**Fig. 4** Stress–strain curves of PU samples post-cured for 2 h

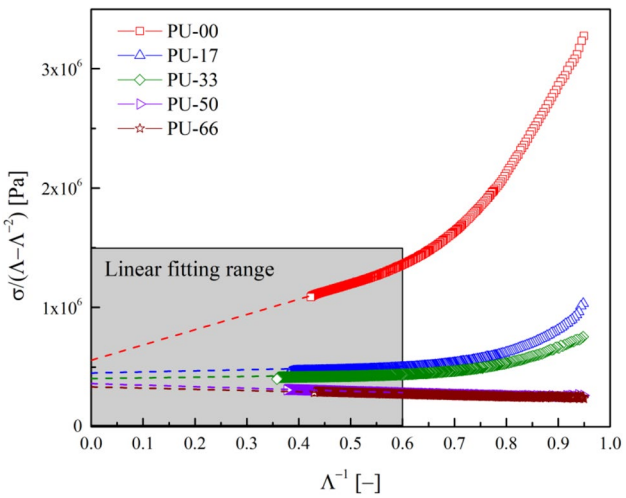


**Fig. 5** Mooney–Rivlin plots for PU samples with the use of the strain amplification factor X. Dash lines are linear extrapolation to intercept

**Table 4** Crosslink density of PU samples

| PRs | Storage modulus at equilibrium state ($G'_e$) | Crosslink density ($n_{G'}$) | Mooney–Rivlin constant ($C_1$) | Crosslink density ($n_{C_1}$) |
|---|---|---|---|---|
| Unit | [Pa] | [mol/m$^3$] | [Pa] | [mol/m$^3$] |
| PR-00 | $1.65\times10^6$ | 655 | $2.79\times10^5$ | 110 |
| PR-17 | $9.48\times10^5$ | 376 | $2.25\times10^5$ | 89 |
| PR-33 | $6.45\times10^5$ | 256 | $2.02\times10^5$ | 80 |
| PR-50 | $3.67\times10^5$ | 145 | $1.81\times10^5$ | 71 |
| PR-66 | $2.27\times10^5$ | 90 | $1.68\times10^5$ | 66 |

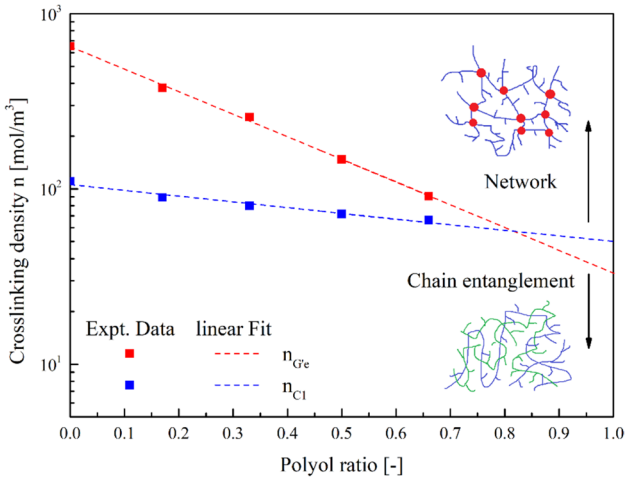


**Fig. 6** Comparison of crosslink density obtained from rheological (red) and tensile measurements (blue). The shadows demonstrate the estimated entanglement density of linear chains from rheological (red) and tensile measurements (blue), respectively

The results of the crosslink density of all PRs obtained from both methods are shown in Table 4. By using Eq. (13) and (16), the crosslink densities of PU-00 to PU-66 are calculated and compared in Fig. 6. The experimental data are fitted by the exponential decay equation.

From the estimation, the crosslink density at the PR of 0.8 calculated by the two methods is relatively similar, with crosslink densities of 63 mol/m$^3$, respectively. However, the crosslink density for lower PR obtained by the tensile test is lower than the crosslink density obtained by the shear test, which is consistent with the results of Hagen et al. (1996).

## Conclusion

In this work, five PU materials with different polyol ratios were synthesized and post-cured. The gel time during the curing reaction was measured by the TRMS method in the rheometer and the Winter–Chambon criterion was used for analysis. TRMS is an appropriate method to estimate and compare gel time, but for these samples with relatively low reaction rates, gel time is only a time range close to the gel point. It was found that the gel time first decreased and then increased with increasing polyol ratio. The gelation times ranged from 231 to 378 min.

In addition, the crosslinking degree of the sample with curing for 24 h in the rheometer was calculated based on the theory of rubber elasticity, and the results were compared with tensile measurement data. Both rheological methods and tensile tests allow an estimation of the crosslink density. However, the crosslink densities obtained from tensile tests were found to be lower than those from the rheological data. Crosslink density reflects the change in structure with the increase in polyol ratio. These results show that gradient properties can be achieved by adjusting the polyol ratio and provide reference information for the liquid additive manufacturing of PU elastomers.

**Supplementary Information** The online version contains supplementary material available at https://doi.org/10.1007/s00397-024-01451-1.

**Acknowledgements** The authors would like to thank the German Research Foundation (DFG) for financial support of this project by grant DFG Wa 668/332, BASF Polyurethanes GmbH for providing the samples and the Open Access Publication Fund.

**Funding** Open Access funding enabled and organized by Projekt DEAL.

**Data Availability** The authors confirm that the data are available within the article and its supplementary materials.

## Declarations

**Conflict of interest** The authors declare no competing interests.



## References

Arrigo R, Mascia L, Clarke J, Malucelli G (2020) Structure evolution of epoxidized natural rubber (ENR) in the melt state by time-resolved mechanical spectroscopy. Materials 13(4):946. https://doi.org/10.3390/ma13040946

Bayer O (1947) Das Di-Isocyanat-Polyadditionsverfahren (Polyurethane). Angew Chem 59(9):257–272. https://doi.org/10.1002/ange.19470590901

Djabourov M, Nishinari K (2013) Ross-Murphy S B. Cambridge University Press, Physical gels from biological and synthetic polymers

Elwell MJ, Ryan AJ, Grünbauer HJM, van Lieshout HC (1996) An FT i.r. study of reaction kinetics and structure development in model flexible polyurethane foam systems. Polymer 37(8):1353–1361. https://doi.org/10.1016/0032-3861(96)81132-3

Flory PJ (1941) Molecular size distribution in three dimensional polymers. II. Trifunctional branching units. J Am Chem Soc 63(11):3091–3096. https://doi.org/10.1021/ja01856a062

Hagen R, Salmén L, Stenberg B (1996) Effects of the type of crosslink on viscoelastic properties of natural rubber. J Polym Sci, Part b: Polym Phys 34(12):1997–2006. https://doi.org/10.1002/(SICI)1099-0488(19960915)34:12%3c1997::AID-POLB5%3e3.0.CO;2-N

Hu X, Fan J, Yue CY (2001) Rheological study of crosslinking and gelation in bismaleimide/cyanate ester interpenetrating polymer network. J Appl Polym Sci 80(13):2437–2445. https://doi.org/10.1002/app.1350

Huang SH, Liu P, Mokasdar A, Hou L (2013) Additive manufacturing and its societal impact: a literature review. Int J Adv Manuf Technol 67(5–8):1191–1203. https://doi.org/10.1007/s00170-012-4558-5

Jandyal A, Chaturvedi I, Wazir I, Raina A, Ul Haq MI (2022) 3D printing – a review of processes, materials and applications in industry 4.0. Sustain Oper Comput 3:33–42. https://doi.org/10.1016/j.susoc.2021.09.004

Jiang H, Su W, Mather PT, Bunning TJ (1999) Rheology of highly swollen chitosan/polyacrylate hydrogels. Polymer 40(16):4593–4602. https://doi.org/10.1016/S0032-3861(99)00070-1

Kruse M, Wagner MH (2016) Time-resolved rheometry of poly(ethylene terephthalate) during thermal and thermo-oxidative degradation. Rheol Acta 55(10):789–800. https://doi.org/10.1007/s00397-016-0955-2

Kruse M (2017) From linear to long-chain branched poly (ethylene terephthalate)–reactive extrusion, rheology and molecular characterization. Dissertation, Technische Universitaet Berlin. https://api-depositonce.tu-berlin.de/server/api/core/bitstreams/9839a102-7e8e-4636-868a-10ca2804edc8/content

Laukkanen O-V, Winter HH, Seppälä J (2018) Characterization of physical aging by time-resolved rheometry: fundamentals and application to bituminous binders. Rheol Acta 57(11):745–756. https://doi.org/10.1007/s00397-018-1114-8

Mortimer S, Ryan AJ, Stanford JL (2001) Rheological behavior and gel-point determination for a model Lewis acid-initiated chain growth epoxy resin. Macromolecules 34(9):2973–2980. https://doi.org/10.1021/ma001835x

Mours M, Winter HH (1994) Time-resolved rheometry. Rheol Acta 33(5):385–397. https://doi.org/10.1007/BF00366581

Mullins L, Tobin NR (1965) Stress softening in rubber vulcanizates. Part I. Use of a strain amplification factor to describe the elastic behavior of filler-reinforced vulcanized rubber. J Appl Polym Sci 9(9):2993–3009. https://doi.org/10.1002/app.1965.070090906

Nakajima-Kambe T, Shigeno-Akutsu Y, Nomura N, Onuma F, Nakahara T (1999) Microbial degradation of polyurethane, polyester polyurethanes and polyether polyurethanes. Appl Microbiol Biotechnol 51(2):134–140. https://doi.org/10.1007/s002530051373

Osswald T, Rudolph N (2015) Polymer rheology. München. https://www.hanser-fachbuch.de/fachbuch/artikel/9781569905173

Rubinstein M, Colby RH (2003) Polymer physics. New York. https://global.oup.com/academic/product/polymer-physics-9780198520597?cc=de&lang=en&

Salehiyan R, Malwela T, Ray SS (2017) Thermo-oxidative degradation study of melt-processed polyethylene and its blend with polyamide using time-resolved rheometry. Polym Degrad Stab 139:130–137. https://doi.org/10.1016/j.polymdegradstab.2017.04.009

Salehiyan R, Bandyopadhyay J, Ray SS (2019) Mechanism of thermal degradation-induced gel formation in polyamide 6/ethylene vinyl alcohol blend nanocomposites studied by time-resolved rheology and hyphenated thermogravimetric analyzer Fourier transform infrared spectroscopy mass spectroscopy: synergistic role of nanoparticles and maleic-anhydride-grafted polypropylene. ACS Omega 4(5):9569–9582. https://doi.org/10.1021/acsomega.9b00940

Saville B, Watson AA (1967) Structural characterization of sulfur-vulcanized rubber networks. Rubber Chem Technol 40(1):100–148. https://doi.org/10.5254/1.3539039

Schäfer K, Nestler D, Tröltzsch J, Ireka I, Niedziela D, Steiner K, Kroll L (2020) Numerical studies of the viscosity of reacting polyurethane foam with experimental validation. Polymers 12(1):105. https://doi.org/10.3390/polym12010105

Sekkar V, Narayanaswamy K, Scariah KJ, Nair PR, Sastri KS, Ang HG (2007) Evaluation by various experimental approaches of the crosslink density of urethane networks based on hydroxyl-terminated polybutadiene. J Appl Polym Sci 103(5):3129–3133. https://doi.org/10.1002/app.24751

Somarathna HMCC, Raman SN, Mohotti D, Mutalib AA, Badri KH (2018) The use of polyurethane for structural and infrastructural engineering applications: a state-of-the-art review. Constr Build Mater 190:995–1014. https://doi.org/10.1016/j.conbuildmat.2018.09.166

Spathis GD (1991) Polyurethane elastomers studied by the Mooney-Rivlin equation for rubbers. J Appl Polym Sci 43(3):613–620. https://doi.org/10.1002/app.1991.070430323

Takeda S, Ohashi M, Kuwano O, Kameda M, Ichihara M (2020) Rheological tests of polyurethane foam undergoing vesiculation-deformation-solidification as a magma analogue. J Volcanol Geoth Res 393:106771. https://doi.org/10.1016/j.jvolgeores.2020.106771

Tung CM, Dynes PJ (1982) Relationship between viscoelastic properties and gelation in thermosetting systems. J Appl Polym Sci 27(2):569–574. https://doi.org/10.1002/app.1982.070270220

Wang P, Auhl D, Uhlmann E, Gerlitzky G, Wagner MH (2019) Rheological and mechanical gradient properties of polyurethane elastomers for 3D-printing with reactive additives. Applied Rheology 29(1):162–172. https://doi.org/10.1515/arh-2019-0014

Winter HH (1987) Can the gel point of a cross-linking polymer be detected by the G′ – G″ crossover? Polym Eng Sci 27(22):1698–1702. https://doi.org/10.1002/pen.760272209

Winter HH (2016) Gel point. In: Mark HF (ed) Encyclopedia of Polymer Science and Technology. Wiley, pp 1–15

Winter HH, Mours M (2006) The cyber infrastructure initiative for rheology. Rheol Acta 45(4):331–338. https://doi.org/10.1007/s00397-005-0041-7

Winter HH, Morganelli P, Chambon F (1988) Stoichiometry effects on rheology of model polyurethanes at the gel point. Macromolecules 21(2):532–535. https://doi.org/10.1021/ma00180a048